J Braz. Soc. Mech. Sci. Eng. (2015) 37:1555–1567
DOI 10.1007/s40430-014-0293-1

TECHNICAL PAPER

Active angular control of a sectioned airfoil using shape memory alloys and fuzzy controller

Gustavo Luiz Chagas Manhães de Abreu · Marcelo F. Maesta · Vicente Lopes Junior · Carlos De Marqui Junior · Cassio T. Faria · Daniel J. Inman

Received: 17 August 2014 / Accepted: 2 December 2014 / Published online: 20 December 2014

Abstract The present work illustrates an example of shape memory alloys and fuzzy controllers applied to active angular control of a sectioned airfoil. The main objective of the proposed control system is to modify the camber line of an airfoil based on the relative rotation between the different sections of the profile, given a reference angle. The changes of the sectioned airfoil angle result from the contraction/expansion of the shape memory alloy caused by heating of the wire with an electric current that changes its temperature by the Joule effect. Considering the presence of plant's nonlinear effects, especially in the mathematical model of the alloy, this work proposes the application of a control system based on fuzzy logic theory. Through numerical and experimental tests, the performance of the fuzzy controller is compared with an on–off controller applied in an airfoil.

Keywords Active angular control · Sectioned airfoil · Fuzzy logic · Shape memory alloys

Technical Editor: Marcelo A. Savi.

G. L. C. M. de Abreu (✉) · M. F. Maesta · V. Lopes Junior
Univ Estadual Paulista, UNESP, Ilha Solteira, SP, Brazil
e-mail: gustavo@dem.feis.unesp.br

C. De Marqui Junior
Departamento de Engenharia Aeronáutica, Universidade de São Paulo, USP, São Carlos, SP, Brazil

C. T. Faria · D. J. Inman
Department of Aerospace Engineering, University of Michigan, Ann Arbor, MI 48109, USA

1 Introduction

The observation of flight in nature has motivated the human desire to fly, and ultimately the development of aircraft. The designs of the first flying machines were relatively crude and even today nature has much to teach us and continuously inspires research.

In just a century, engineers built aircraft that can travel above the sound speed, cross the circumference of the earth without refueling and even cross the atmosphere into space. It is desired to have aircraft that are able to rapidly change shape to transition from efficient cruise to aggressive maneuvering and precision descents. There are specific geometric features required (for example: curvature of the wings) that allow aircraft to achieve maximum flight efficiency successfully.

Incorporating morphing structures into aircraft is not a new idea. In fact, the first powered aircraft to take flight, the Wright Flyer, was based on a wing design intended to smoothly deform or morph. In the last couple of decades, advances in materials have made it feasible to create robust morphing aerospace structures that allow aircraft to fly for a variety of flight regimes. The ability of a wing surface to change its geometry during flight has interested researchers and designers over the years. An adaptive wing diminishes the compromises required to insure the operation of the airplane in multiple flight conditions [23]; [5]).

Several mechanisms are proposed to create an adaptive wing aircraft [1] and the main difficulty of trying to create such system is to find lightweight and efficient actuators that are capable of providing sufficient force and deform evenly. A synthetic material that has this characteristic is the shape memory alloy (SMA) [2]. This material is capable of converting thermal energy into mechanical energy and once deformed the material can return to its original

shape by heating. This phenomenon is known as the shape memory effect, and it occurs due to a temperature and stress dependent shift in the material's crystalline structure between martensite and austenite phases [11].

Shape memory alloy actuators have several advantages such as excellent power-to-mass ratio, maintainability, reliability, and clean and silent actuation. The disadvantages are low energy efficiency due to conversion of heat to mechanical energy, inaccurate motion control due to hysteresis, nonlinearities, parameter uncertainties, difficulty in measuring variables such as temperature, and slow response due to the thermal process involved in the working principle [21].

In an ongoing effort to increase the efficiency and capability of modern aircraft, SMAs are being implemented in both novel applications and the replacement of conventional devices with alternatives that are more compact, more powerful, and less complicated [25]. Although SMA actuators show potential in morphing applications, there is still no feasible solution due to structural constraint and difficulty in controlling the nonlinear actuators. Martin et al. [17] provided a detailed description of the design, integration, and testing of an experimental study of a wingbox actuated by SMA wires. Lv et al. [16] developed an SMA torsion actuator based on NiTi wires and a thin-walled tube for an adaptive wing demonstration system. Sofla et al. [22] proposed a wing that deforms to target shapes by actuating the wingbox using SMAs. The prototypes showed excellent and smooth movement under representative loads. Bil et al. [3] developed an adaptive airfoil control system demonstrator using SMA actuators. Three types of controllers were tested (conventional PID, PID with robust compensator and PID with anti-windup compensator) in both simulation and in wind tunnel tests. The performance of each controller was determined by its ability to respond and track a required level of morphing. In addition, the effect of ambient temperature due to flying at altitude and power levels required to overcome aerodynamic forces were also determined [19, 20].

In the literature, it has been shown that fuzzy logic control is robust in controlling nonlinear systems [11]. Fuzzy controllers are most suitable for systems that cannot be precisely described by mathematical formulations [26]. In this case, a control designer captures the operator's knowledge and converts it into a set of fuzzy control rules. Fuzzy logic is useful for representing linguistic terms numerically and making reliable decisions with ambiguous and imprecise events or facts. The benefit of the simple design procedure of a fuzzy controller has led to the successful application of a variety of engineering systems [13].

Due to presence of nonlinear effects, especially in the mathematical model of the SMA [4], this paper proposes an active angular control system based on fuzzy logic theory [6] applied to a sectioned airfoil with SMA wires. One obvious issue is that the system exhibits highly nonlinear behavior and some of the system parameters are unknown and/or environment-dependent [11]. Fuzzy control has the advantages of being robust to disturbances and reduces the design complexity for control problems untreatable by classical techniques [8–10, 12, 14, 24].

This work focuses on the design, implementation and experimental test of active angular control of a particular sectioned airfoil actuated by a pair of SMA wires. The profile consists of a NACA-0012 model mounted to a base plate and has approximately 500 mm chord. By using a rotary potentiometer as a feedback sensor and a pair of SMAs as actuators, a fuzzy controller is designed to control the profile angle actively. The control system consists of independent SISO loops, i.e. decentralized active angular control with local fuzzy controllers. A dSPACE digital data acquisition and real-time control system along with Matlab Simulink® is used to implement the controller in real time. Experimental results show that the pair of SMA actuators can effectively control the profile angle by using the fuzzy logic controller.

The organization of the paper is as follows: The next section presents a description of the actuation mechanism (a pair of SMA wires) of the proposed sectioned airfoil, along with the mathematical model for the system. Section 4 describes the theoretical concepts and the main features of the fuzzy controller implemented here. In Sects. 5 and 6, respectively, the numerical simulations and experimental tests with both fuzzy and on–off controllers are performed in order to compare and verify the performance of the proposed fuzzy control system. Finally, concluding remarks are presented.

2 Actuation mechanism description and mathematical modeling

Figure 1 shows a schematic sectioned airfoil with a pair of SMA wires. The profile consists of a NACA-0012 model and has approximately 500 mm chord. By using a pair of

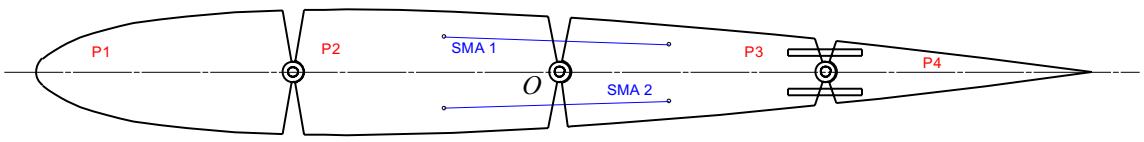

Fig. 1 Schematic drawing of the sectioned airfoil with SMA wires

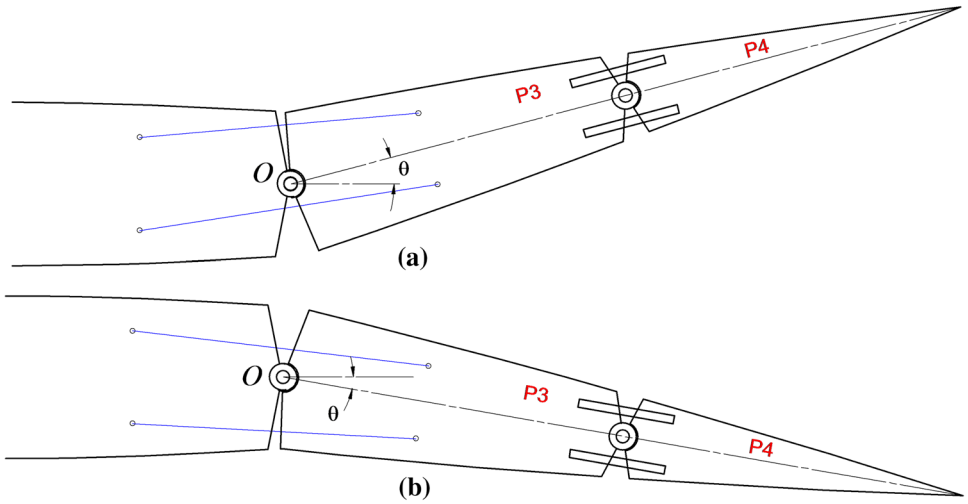

Fig. 2 Behavior of the sectioned airfoil when **a** SMA 1 is heated and **b** SMA 2 is heated

SMAs as actuators, a fuzzy controller is designed to control the profile angle actively [7].

According to Faria et al. [7], Bil et al. [3] and Pankonien et al. [19], SMA wires can induce large force and displacements when the temperature is changed, which make it potential actuator for a wing morphing system. In this work, the SMA wires were fixed in this particular profile to maximize the acting moments around the articulation point O.

In future studies, all sections will be considered. Since the model presented in this work is not just a system of one degree of freedom, only the central articulation was driven using a pair of SMA wire. In this model, each SMA actuator used was NiTinol wire. As shown in Fig. 1, the angular position of the sectioned airfoil was measured by a rotary potentiometer positioned between sections $P2$ and $P3$.

According Fig. 2, when one of the wires is heated, it contracts and induces tension in the other SMA wire and the airfoil (sections $P3$ and $P4$) rotates around point O.

When the second wire is heated, its contraction will result in the extension of the opposing SMA actuator mechanically. Thus it recovers the strain and moves the sectioned airfoil in the opposite direction. The position of the profile is determined by heating and cooling the two SWA wires. By heating one of the wires in an initially deformed state, a reduction in wire length due to transformation strain in the SMA will create a relative rotation between airfoil parts ($P3$ and $P4$) while straining the opposite, cooling wire. After the actuation is complete and the desired angular position is reached, no additional energy is required to maintain the deformed shape. The purpose of the system is to force the rotation angle θ of the profile to follow the desired trajectory θ_d.

The mathematical model of the system is composed of a thermal model, a phase transformation model, and a description of the system dynamics.

2.1 Thermal model

SMA actuators are most commonly used in a wire form and electrical heating commonly induces the phase transformation. In the conventional method of actuation, each SMA wire is continuously heated by electric current [4].

A common model of the heat transfer associated with electrical heating (also known as Joule heating) of the wire is [15]:

$$(\rho A)c_p\frac{dT(t)}{dt} = \frac{V^2}{R_w} - h_c A_c[T(t) - T_\infty] \tag{1}$$

where ρ is the density of the shape memory material, A is the cross-sectional area ($A = \pi d^2/4$, where d is the diameter of the wire), c_p is the specific heat of the wire and R_w is the resistance per unit length of the material. The parameter h_c is the natural convective heat transfer coefficient and A_c is the circumferential area of the unit length of wire ($A = \pi d$). The ambient temperature is denoted T_∞ and the electric voltage V across the SMA wire is the control variable of the system.

Assuming that the voltage is constant and the initial temperature is equal to the ambient temperature, the solution to this differential Eq. (1) is

$$T(t) = T_\infty + \frac{1}{R_w h_c A_c}\left(1 - e^{-t/t_h}\right)V^2 \tag{2}$$

where $t_h = \frac{\rho A c_p}{h_c A_c}$ is defined as time constant associated with the heat transfer process.

In this model, the ambient temperature is assumed constant and only the convective effects are considered. It is also assumed that the temperature (T) is uniform along the wire's length and the SMA wire has an average electrical resistance (R_w), i.e., the variation of the electrical resistance during the phase transformation is neglected.

2.2 Phase transformation

The SMA model used in the numerical simulations is derived by Brinson [4]. This particular model was chosen due to its excellent accuracy between the simulation and experimental results, which clearly justify the use of the model for describing the transformation between martensite (M) and austenite (A) phases [18]. This model replicates the behavior of the SMA at the phenomenological level. During heating, the transformation occurs from martensite to austenite, and during the cooling phase, the opposite transformation occurs.

The SMA constitutive model defines the thermomechanical characteristics of the material, i.e. the effect of the temperature on the stress as the SMA undergoes phase transformation [11]. The relationships between stress (σ), strain (ε), temperature and martensite fraction within the SMA wire during phase transformation (ξ) can be defined as [4]:

$$\dot{\sigma} = D\dot{\varepsilon} + \Theta\dot{T} + \Omega\dot{\xi} \tag{3}$$

where D is Young's modulus of the alloy, Θ is the thermo-elastic factor, Ω is the phase transformation coefficient and $\xi = \xi_s + \xi_T$ is decomposed further into a summation of two variables: ξ_s is the fraction of stress-induced martensite in the material and ξ_T is the fraction of temperature-induced martensite in the material.

Brinson [4] demonstrated that despite the thermo-elastic effect one can obtain the following relation based on Eq. (3), considering ε_L as the maximum strain that can be recovered through the transformation phase:

$$\sigma = D(\xi)[\varepsilon - \varepsilon_L \xi_s] \tag{4}$$

where the actual Young's modulus $D(\xi)$ is assumed to be a linear function of the martensite fraction: $D(\xi) = D_A + \xi(D_M - D_A)$, and D_A and D_M are, respectively, the elastic modulus in the austenite and martensite state.

According to Brinson [4], the transformation equations also require modification to account for the transformation between the different types of martensite. The kinetic law for conversion from martensite to austenite is:For $T > M_s$ and $C_A(T - A_f) < \sigma < C_A(T - A_s)$:

$$\xi = \frac{\xi_0}{2}\left\{\cos\left[a_A\left(T - A_s - \frac{\sigma}{C_A}\right)\right] + 1\right\},$$
$$\text{where } \xi_{S,T} = \xi_{S0,T0} - \frac{\xi_{S0,T0}}{\xi_0}(\xi_0 - \xi). \tag{5}$$

The kinetic laws of transformation from austenite to martensite become more elaborate, because the fraction of stress- and temperature-induced martensite must also be computed during the process. For temperatures above M_s and $\sigma_s^{cr} + C_M(T - M_s) < \sigma < \sigma_f^{cr} + C_M(T - M_s)$:

$$\xi_S = \frac{1 - \xi_{S0}}{2}\cos\left\{\frac{\pi}{\sigma_s^{cr} - \sigma_f^{cr}} \times \left[\sigma - \sigma_f^{cr} - C_M(T - M_s)\right]\right\} + \frac{1 + \xi_{S0}}{2}$$
$$\xi_T = \xi_{T0} - \frac{\xi_{T0}}{1 - \xi_{S0}}(\xi_S - \xi_{S0}) \tag{6}$$

where C_A and C_M are material properties that describe the relationship of temperature and the critical stress at the start (σ_s^{cr}) and finish (σ_f^{cr}) of the conversion of the martensite variants; ξ_{S0} and ξ_{T0} are the initial martensite fractions; A_s and A_f are the initial and final temperature of austenite transformation, respectively; M_s and M_f are the initial and final temperature of martensite transformation, respectively.

For temperatures below M_s and $\sigma_s^{cr} < \sigma < \sigma_f^{cr}$:

$$\xi_S = \frac{1 - \xi_{S0}}{2}\cos\left[\frac{\pi}{\sigma_s^{cr} - \sigma_f^{cr}}\left(\sigma - \sigma_f^{cr}\right)\right] + \frac{1 + \xi_{S0}}{2}$$
$$\xi_T = \xi_{T0} - \frac{\xi_{T0}}{1 - \xi_{S0}}(\xi_S - \xi_{S0}) + \Delta_{T\xi}. \tag{7}$$

The variable $\Delta_{T\xi}$ is defined as

$$\Delta_T = \frac{1 - \xi_{T0}}{2}\{\cos[a_M(T - M_f)] + 1\} \tag{8}$$

if $M_f < T < M_s$ and $T < T_0$. Otherwise, $\Delta_{T\xi} = 0$, where $a_M = \frac{\pi}{M_s - M_f}$ and $a_A = \frac{\pi}{A_f - A_s}$.

2.3 System dynamics

As shown in Fig. 3a, the inertial frame *O-XY* of the airfoil profile is centered at point *O*. The control objective consists in forcing the profile to track a specified angular trajectory. The trajectory is defined in the plane coordinate system frame *O-xy*. Observe that it is a moving frame and the position and orientation of the profile (*P*3 and *P*4 parts) are associated to the sectioned airfoil's initial configuration.

The position vector of points *A*, *B*, *C* and *D* (SMA wire connections) with respect the frame *O-XYZ* is defined, respectively, as:

$$\vec{r}_{OA} = \begin{bmatrix} -a_1 \\ a_2 \\ 0 \end{bmatrix}; \quad \vec{r}_{OB} = R^T \begin{bmatrix} b_1 \\ b_2 \\ 0 \end{bmatrix} \vec{r}_{OC} = \begin{bmatrix} -c_1 \\ -c_2 \\ 0 \end{bmatrix}$$
$$\text{and } \vec{r}_{OD} = R^T \begin{bmatrix} d_1 \\ -d_2 \\ 0 \end{bmatrix} \tag{9}$$

where R is the rotation matrix from inertial (X, Y, Z) to moving frame (x, y, z):

$$R = \begin{bmatrix} \cos\theta & \sin\theta & 0 \\ -\sin\theta & \cos\theta & 0 \\ 0 & 0 & 1 \end{bmatrix}. \tag{10}$$

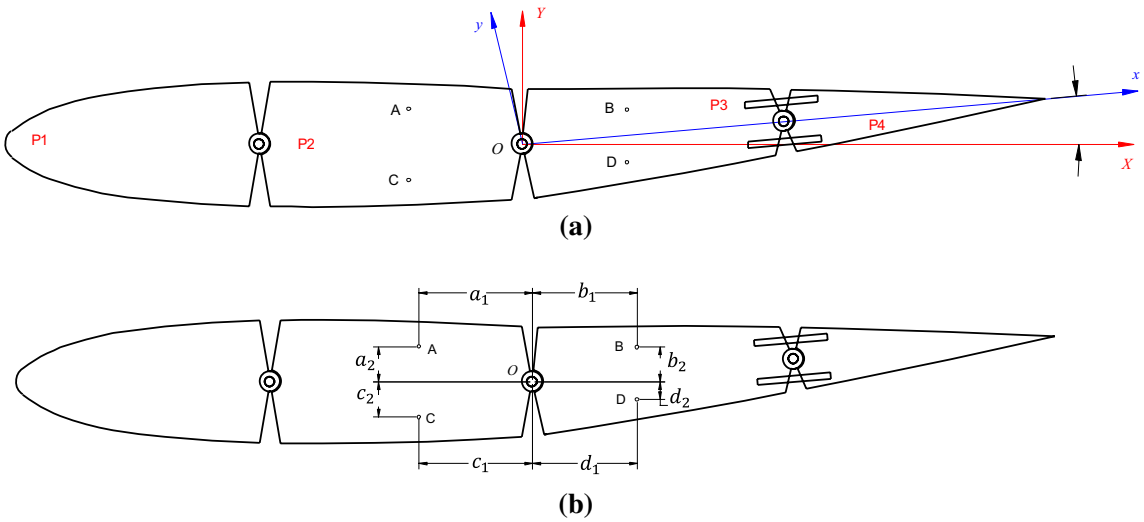

Fig. 3 **a** Inertial (*XY*) and non-inertial (*xy*) reference axes and **b** SMA wire connection point positions

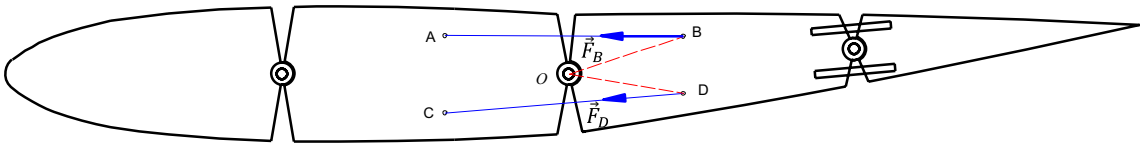

Fig. 4 External forces acting on the sectioned airfoil

Finally, the length of each SMA wire ($\vec{r}_{AB}$ and $\vec{r}_{CD}$) are defined as follows:

$$\vec{r}_{AB} = \vec{r}_{AO} + \vec{r}_{OB} = \begin{bmatrix} b_1\cos\theta - b_2\sin\theta + a_1 \\ b_1\sin\theta + b_2\cos\theta - a_2 \\ 0 \end{bmatrix} \tag{11a}$$

$$\vec{r}_{CD} = \vec{r}_{CO} + \vec{r}_{OD} = \begin{bmatrix} d_1\cos\theta + d_2\sin\theta + c_1 \\ d_1\sin\theta - d_2\cos\theta + c_2 \\ 0 \end{bmatrix} \tag{11b}$$

Therefore, according to Fig. 4, the external forces applied to the points *B* and *D* with respect to the frame *O-XYZ* are given by:

$$\vec{F}_B = F_{AB}\frac{\vec{r}_{AB}}{||\vec{r}_{AB}||} \tag{12a}$$

$$\vec{F}_D = F_{CD}\frac{\vec{r}_{CD}}{||\vec{r}_{CD}||} \tag{12b}$$

where $||\ ||$ denotes the modulus of a vector, F_{AB} and F_{CD} are the generated forces due to the stresses (σ) in the SMA wires (Eq. 4) and thus can be described as: $F_{AB} = \sigma_{AB}A$ and $F_{CD} = \sigma_{CD}A$, where A is the cross sectional area of the wire (assumed equal for both SMA wires). The maximum strains (ε_L) (Eq. 4) for both SMA wires are derived as follows:

$$\varepsilon_L^{AB} = \frac{||\vec{r}_{AB}||_{\theta_{min}} - ||\vec{r}_{AB}||_{\theta_{max}}}{||\vec{r}_{AB}||_{\theta_{max}}} \tag{13a}$$

$$\varepsilon_L^{CD} = \frac{||\overrightarrow{r}_{CD}||_{\theta_{min}} - ||\overrightarrow{r}_{CD}||_{\theta_{max}}}{||\overrightarrow{r}_{CD}||_{\theta_{max}}} \tag{13b}$$

where θ_{min} and θ_{max} are respectively, the maximum and minimum angle of the sectioned airfoil.

The acting moments applied in points *B* and *D* are defined as:

$$\vec{M}_B = \vec{r}_{OB} \times \vec{F}_B \tag{14a}$$

$$\vec{M}_D = \vec{r}_{OD} \times \vec{F}_D \tag{14b}$$

Substituting Eqs. (12a, 12b) and (9) in (14a, 14b) yields:

$$\vec{M}_B = \frac{F_{AB}}{||\vec{r}_{AB}||}(a_1b_2\cos\theta + a_2b_1\cos\theta + a_1b_1\sin\theta - a_2b_2\sin\theta) \tag{15a}$$

$$\vec{M}_D = \frac{F_{CD}}{||\vec{r}_{CD}||}(c_1d_1\sin\theta - c_2d_1\cos\theta - c_1d_2\cos\theta - c_2d_2\sin\theta). \tag{15b}$$

Then the resulting equation of angular motion for the sectioned airfoil is given by:

$$J\ddot{\theta} + \alpha\dot{\theta} = \vec{M}_B + \vec{M}_D \tag{16}$$

where J is the moment of inertia of parts $P3$ and $P4$, and α is the dynamic friction coefficient in articulation point O.

In the experimental tests, two methods for controlling SMAs, without using complex mathematical models, were tested and compared. The first one is a simple Bang–Bang controller that activates each SMA wire until the desired angular position is reached. The second one consists of a rule-based controller that activates each SMA individually depending on the proximity of the airfoil to the desired angular position. The latter takes into account the error of the angular position (E) as well as the rate of change of that error with respect to time ($\mathrm{d}E/\mathrm{d}t$). A detailed description of the rule-based controller is presented in the following section.

3 Controller design

The design of a conventional Fuzzy Logic Controller (FLC) consists of three main steps [6]: (1) fuzzification of input and output variables using sets of membership functions, (2) development of fuzzy control rules and (3) defuzzification of output membership values.

3.1 Fuzzification

Figure 5 shows seven equally spaced triangular membership functions that were employed to convert the input variables (the angular error E and angular error derivative $\mathrm{d}E/\mathrm{d}t$) and output variable (applied electric voltage V) into linguistic fuzzy variables.

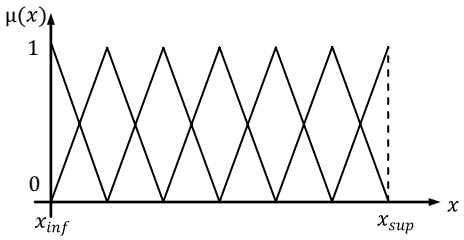

Fig. 5 A set of membership functions used for input and output variables

The labels or membership functions try to translate verbally the meaning of a specific variable in its universe of discourse. For input variable $\mathrm{d}E/\mathrm{d}t$, each membership function was assumed as: "Negative Large" (NL), "Negative Medium" (NM), "Negative Small" (NS), "Zero" (Z), "Positive Small" (PS), "Positive Medium" (PM) and "Positive Large" (PL). For the input variable E: Z, $E1$, $E2$, $E3$, $E4$, $E5$ and $E6$ (for *SMA* 1); $E6$, $E5$, $E4$, $E3$, $E2$, $E1$ and Z (for SMA 2) and for the output V: Z, $V1$, $V2$, $V3$, $V4$, $V5$ and $V6$.

For the input variables, it is necessary to define the range $[x_{\mathrm{inf}}, x_{\mathrm{sup}}]$ of the input membership functions. In the case of the sectioned airfoil, $[0, 5]$ degrees and $[-5, 0]$ degrees were used as the range of the input membership functions for the angular error (E) to SMA 1 and SMA 2, respectively. The angular error derivative ($\mathrm{d}E/\mathrm{d}t$) varies from $[-5, 5]$ degrees/seconds for both SMAs, and the applied electric voltage V varies from $[0, 6.75]$ Volts.

3.2 Fuzzy control rules

In order to emulate the use of the intuitive knowledge, and to avoid the need of any mathematical models of the SMA actuators, a rule based control system was proposed in the present study. The rule-based controller is essentially a fuzzy logic controller with triangular membership functions.

In this paper, the rule base was built from the intuitive knowledge of the dynamic behavior of the sectioned airfoil considering the electric voltage applied in SMA 1 and SMA 2. The fuzzy control rules that are associated with the fuzzified values of the error (E) and its derivative ($\mathrm{d}E/\mathrm{d}t$) were formulated in order to improve the system response and compensate for the nonlinearities and parametric uncertainties of the individual SMA actuators employed in the system [11]. Tables 1 and 2 give the complete set of the fuzzy control rules for the SMAs 1 and 2 (e.g., for the first rule, when E is Z and $\mathrm{d}E/\mathrm{d}t$ is NL then V is Z). The "max–min" method with the logical operator AND has been used as the inference method.

Table 1 Fuzzy control rules for the SMA 1

		E						
		Z	$E1$	$E2$	$E3$	$E4$	$E5$	$E6$
$\frac{\mathrm{d}E}{\mathrm{d}t}$	NL	Z	$V1$	$V3$	$V3$	$V4$	$V5$	$V5$
	NM	Z	$V2$	$V3$	$V4$	$V5$	$V5$	$V5$
	NS	Z	$V3$	$V4$	$V4$	$V5$	$V6$	$V6$
	Z	Z	$V3$	$V4$	$V5$	$V6$	$V6$	$V6$
	PS	Z	Z	Z	Z	Z	Z	Z
	PM	Z	Z	Z	Z	Z	Z	Z
	PL	Z	Z	Z	Z	Z	Z	Z

Table 2 Fuzzy control rules for the SMA 2

		E						
		$E6$	$E5$	$E4$	$E3$	$E2$	$E1$	Z
$\frac{dE}{dt}$	NL	Z	Z	Z	Z	Z	Z	Z
	NM	Z	Z	Z	Z	Z	Z	Z
	NS	Z	Z	Z	Z	Z	Z	Z
	Z	$V6$	$V6$	$V5$	$V5$	$V4$	$V3$	Z
	PS	$V6$	$V5$	$V5$	$V4$	$V4$	$V3$	Z
	PM	$V5$	$V5$	$V4$	$V4$	$V3$	$V2$	Z
	PL	$V5$	$V5$	$V4$	$V3$	$V3$	$V1$	Z

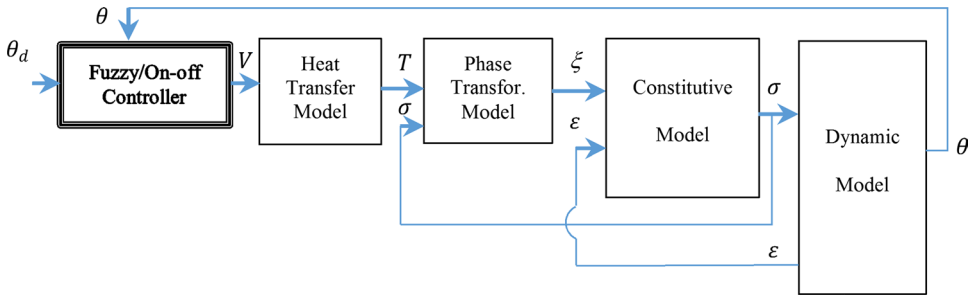

Fig. 6 Overall control block diagram for the sectioned airfoil

As shown in Tables 1 and 2, due to location of the SMA wires in profile, the fuzzy control rules for both wires are similar and have opposite control actions, i.e., as shown in Table 1, when the error is positive (Z, $E1$, $E2$, $E3$, $E4$, $E5$ and $E6$) and its derivative is negative (NL, NM, NS, Z), only the SMA 1 should be activated. Otherwise (see Table 2), when the error is negative ($E6$, $E5$, $E4$, $E3$, $E2$, $E1$ and Z) and its derivative is positive (Z, PS, PM, PL), only the SMA 2 should be activated.

For example, considering the extreme situation where the sectioned airfoil has a large angular error ($E6$) and the variation of the error equal to Z, then the maximum control action ($V6$) applied in SMA 1 or 2 is required to cause the rotation of the profile (clockwise or counterclockwise) for achieving the reference angle quickly. In other situation, when the sectioned airfoil is rotating fast (dE/dt is NL) with a large angular error ($E6$), then a high control voltage ($V5$) is required to maintain the speed rotation of the profile. Otherwise, when the airfoil is rotating very slowly (NS) with a large error ($E6$) then a maximum voltage ($V6$) must be applied in SMA wire to increase the speed of rotation of the sectioned airfoil until it achieves the desired angular value. This intuitive knowledge can be extended to other situations where the profile has smaller input values (E and dE/dt).

The controller is designed to set the activation of each SMA based on the overall configuration of the sectioned airfoil. Based on the angular error E, the control system selects the appropriate activation voltage for each SMA wire according to equation below:

$$V(t) = \begin{cases} V_{\mathrm{SMA1}}(t) & \text{if } E(t) > 0 \\ V_{\mathrm{SMA2}}(t) & \text{if } E(t) < 0 \end{cases} \tag{17}$$

where V_{SMA1} and V_{SMA2} are the electric voltages applied to *SMA* wires 1 and 2, respectively, by using the fuzzy/on–off controllers. In this work, both V_{SMA1} and V_{SMA2} were set to 6.75 V for the on–off controller.

3.3 Defuzzification

The defuzzification, i.e. the transformation of fuzzy set output on a numerical control action, is performed using the centroid method [6].

4 Simulation results

To verify the performance of the proposed controller, the numerical results, obtained from the control of the airfoil at different angular positions, are presented. A simple on–off control scheme is used for comparison. This controller corresponds to the so-called Bang–Bang controller that activates the SMA actuator until the desired angular displacement is reached.

Figure 6 shows a block diagram representation of the overall mathematical model of the system [11], with the added fuzzy/on–off controller. The modeling of the proposed sectioned airfoil system is composed of four parts: the heat transfer model between the SMA wires and the

Table 3 Parameters used for the system model

Parameter	Value	Parameter	Value
d	5.08×10^{-4} m	D_A	67 GPa
ρ	6,450 kg/m^3	D_M	26 GPa
A	2.02×10^{-7}m^2	C_A	13 MPa/°C
A_c	1.6×10^{-3}m^2/m	C_M	8 MPa/°C
h_c	70 W/km^2	M_s	50 °C
T_∞	25 °C	M_f	40 °C
J	1.44×10^{-3}kgm^2	A_s	55 °C
α	2×10^{-3}kgm^2/s	A_f	70 °C
a_1, c_1	54×10^{-3}m	σ_s^{cr}	100 MPa
a_2, c_2	17×10^{-3}m	σ_f^{cr}	170 MPa
b_1, d_1	50×10^{-3}m	R_w	3.75 Ω/m
b_2, d_2	13×10^{-3}m	c_p	837 J/kgK

surrounding environment (Eq. 2); the phase transformation model between the martensite and austenite phases of the wire (Eqs. 5–8); the constitutive model of its thermomechanical characteristics (Eq. 4); as well as the dynamic model of the system that describes the motion of the airfoil profile (Eq. 16).

The physical and geometrical parameters of the model are listed in Table 3. The SMA wire parameters were provided for a NiTinol alloy, whose properties were obtained from Brinson [4].

As depicted in Fig. 3a, the profile was built to move starting with angle of $\theta = 5°$. Because of that, the total motion range was set equally for both wires, i.e., 10° for SMA 1 and −15° for SMA 2. Therefore, the range of motion of the airfoil profile is given by: $[\theta_{\min}, \theta_{\max}] = [-15°, 10°]$. Thus, the maximum strains (ε_L) for both SMA wires (Eqs. 13a, 13b) are given respectively by: $\varepsilon_L^{AB} = 0.0593$ and $\varepsilon_L^{CD} = 0.0703$.

The differential Eq. (16) is solved by using the subroutine *rk*4 given in C^{++} library which implements a simple Runge–Kutta method for an initial value problem. The time step used in solving the differential equation is d$t = 0.1$ s. The sectioned airfoil is initially stretched out with the minimal angular position ($\theta_0 = -15°$). Therefore, at $t = 0$, the material for SMA 1 has no stress-induced or temperature-induced martensite: $\xi_{S0}^1 = 0$ and $\xi_{T0}^1 = 0$, and the material for SMA 2 is assumed to be at a state of zero stress and zero strain ($\xi_{S0}^2 = 1$ and $\xi_{T0}^2 = 0$).

The task consists in forcing the parts *P*3 and *P*4 to track a specified angular trajectory. The main goal of the subsequent tracking tests is to verify the performance of the proposed fuzzy and also the on–off controllers to follow commanded trajectories (θ_d). Figure 7 compares the simulation

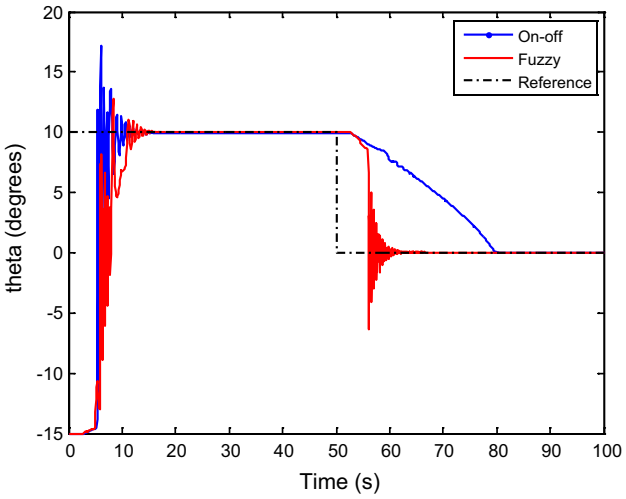

Fig. 7 Angular responses of the sectioned airfoil using fuzzy and on–off controllers

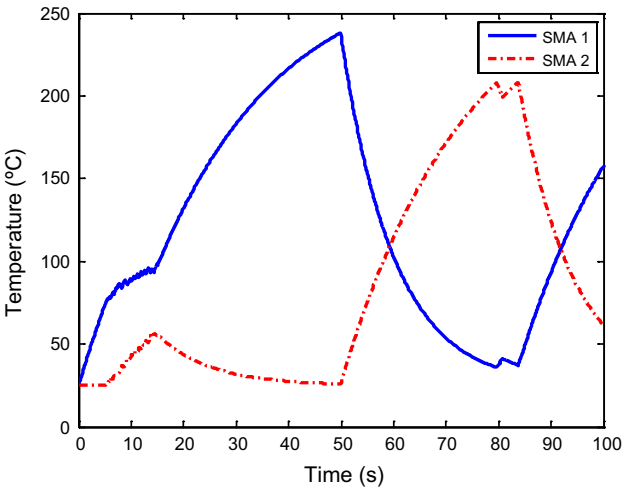

Fig. 8 Temperature responses of the SMA wires using on–off controller

results for the on–off and proposed fuzzy controllers when two input signals (10° and 0°) were given as references (θ_d).

From the analysis of the Fig. 7, the fuzzy controller showed results quite optimistic about minimizing the settling time (66 s), compared with on–off controller (82 s).

Figures 8, 9, 10 and 11 show the temporal evolutions of the temperatures (by using Eq. 2) and martensite fractions of the SMA wires 1 and 2, by using the on–off and fuzzy controllers, respectively.

As can be seen in Figs. 12 and 13, smaller control voltages are obtained using the fuzzy control algorithm.

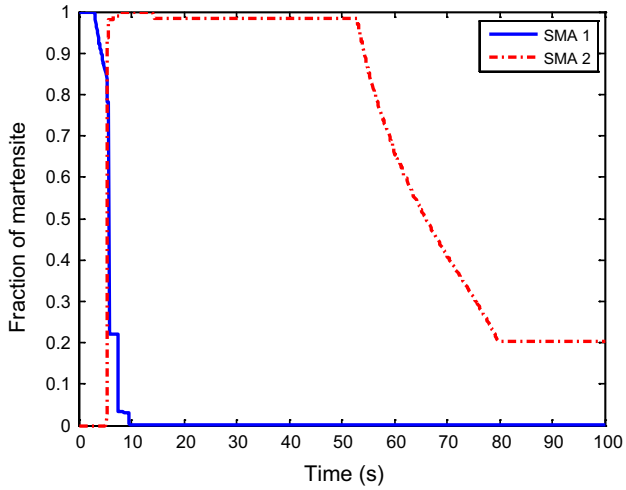

Fig. 9 Fraction of martensite of the SMA wires using on–off controller

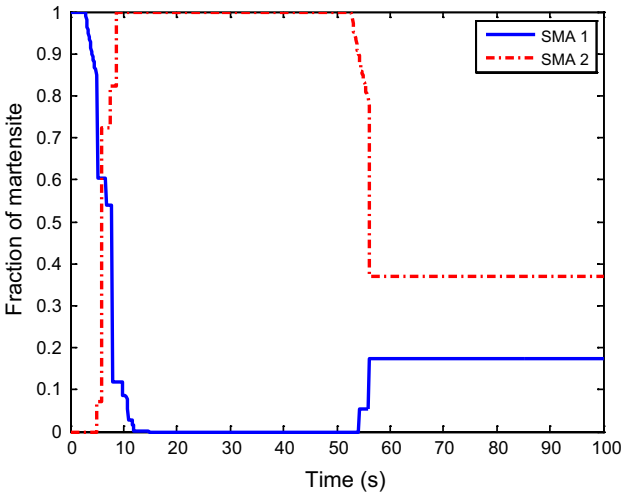

Fig. 11 Fraction of martensite of the SMA wires using fuzzy controller

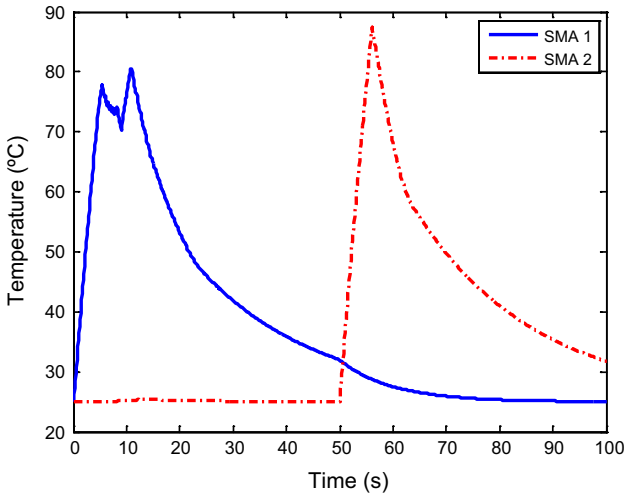

Fig. 10 Temperature responses of the SMA wires using fuzzy controller

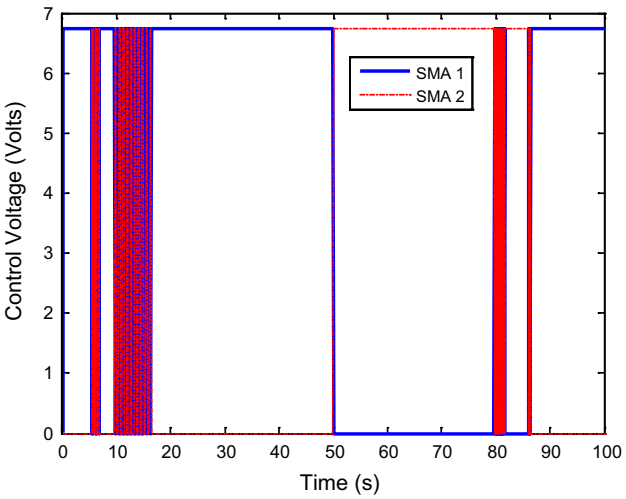

Fig. 12 Control voltage applied to the SMAs actuators using on–off controller

In the case of the on–off controller, the RMS of the control voltage was 5.28 V for SMA 1 and 4.20 V for SMA 2, while in the case of the fuzzy controller, the RMS of the control voltage was only 1.83 V for SMA 1 and 1.72 V for SMA 2.

5 Experimental results

The performance of the fuzzy controller was experimentally tested, in order to verify the angular behavior of the sectioned airfoil using a pair of SMA actuators. Figure 14 shows the setup of the experimental apparatus.

As shown in Fig. 15, the angular position of the sectioned airfoil was measured by a rotary potentiometer positioned between parts $P2$ and $P3$.

According to Fig. 15, the value of the output voltage (V_0) as a function of the angle (θ) of the sensor is given by the following equation:

$$V_0 = a\theta + b \tag{18}$$

where $a = -0.012$ and $b = 2.6$.

The sensor signal was fed to the computer through an *A/D* dSPACE 1103 controller board. The control current applied to each SMA actuator was obtained from a *D/A*

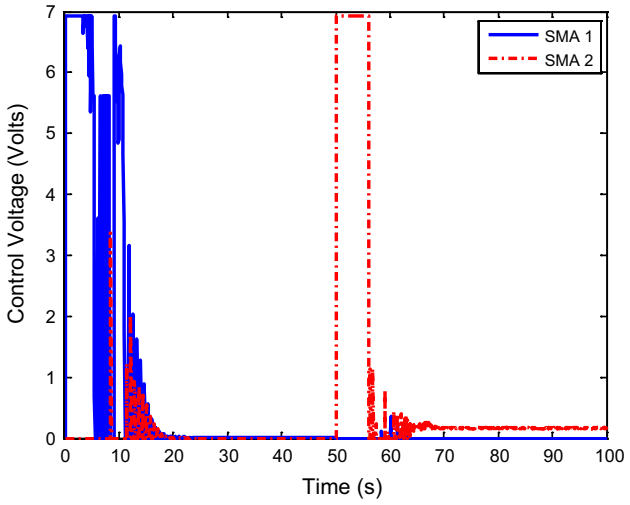

Fig. 13 Control voltage applied to the SMAs actuators using fuzzy controller

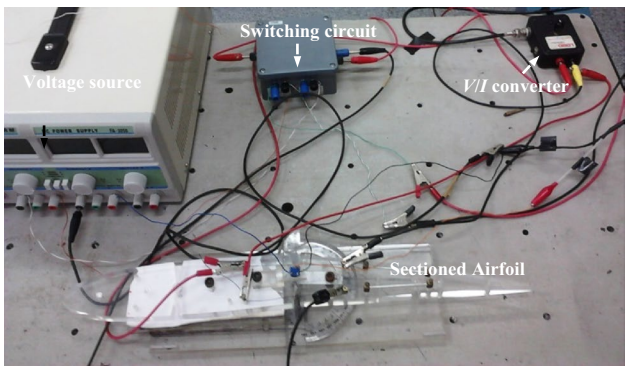

Fig. 14 Setup of the experimental apparatus

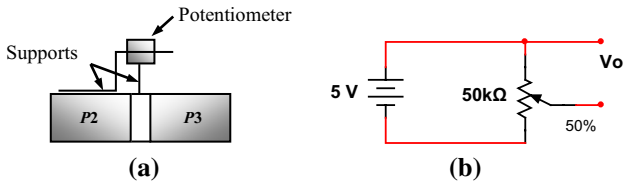

Fig. 15 **a** Sensor location on the profile and **b** equivalent electric circuit

card and a *V*/*I* converter (Lord RD-3002-1). The main specifications of those devices are shown in Table 4. This system was controlled in real-time with Matlab Simulink® software together with a PC and the dSPACE 1103 board. The sampling frequency was set to 1 kHz in all experiments. Finally, a low-pass butterworth analog filter (cut-off frequency of 10 Hz) was used to attenuate the noise effect of the sensor.

A switching circuit was built to change the controller action between the SMAs. Figure 16 shows the schematic diagram.

Matlab Simulink® software was used to acquire and process the data from the potentiometer, and to send the command for the current that must be imposed on the SMA wire. Such software is flexible, and several control algorithms can be easily implemented. Furthermore, all graphical and mathematical tools provided by Matlab Simulink® can be used. The interface with AD/DA dSPACE 1103 board was developed by means of low-level code included in the software. Figures 17 and 18 show, respectively, a Simulink® block diagram of the on–off and fuzzy control systems.

According to the above diagram, from the error signal (E) and its time variation ($\mathrm{d}E/\mathrm{d}t$), the controller (on–off/fuzzy) produces an electrical voltage signal (V) that feeds the current amplifier and drives the actuator SMA 1 or 2, depending on the error signal (E). Then, the angular displacements of the airfoil are captured by the linear potentiometer and then are acquired and filtered. According to Eq. (18) that signals are transformed to degrees and then they are compared to the reference θ_{d} generating the error signal E and its temporal variation ($\mathrm{d}E/\mathrm{d}t$). Thus, the error signal (E) and variation of the angular error ($\mathrm{d}E/\mathrm{d}t$) are fed by the controller and a new output is feedback into the control loop. Finally, to change the controller action between the SMAs, the signal of the on–off/fuzzy controller can take two values (positive or negative) and the corresponding output (0 or 10 V) feeds the switching electric circuit (see Fig. 16).

To verify the controller performance experimentally, open loop and closed loop tests were conducted and the results are presented. Figure 19 shows a sequence of step response plots performed experimentally. The sectioned airfoil initially rotates from the angular position of + 5° to

Table 4 List of experimental devices parameters

Devices	Main parameters
SMA wire	Model: NiTinol, type: Ni–Ti material, Pull actuator length: ≈106 mm, diameter: 0.508 mm
V/*I* converter	Voltage 0–5 V, current 0–2 A
dSPACE 1103 board	*A*/*D* and *D*/*A* 16 bit card
Potentiometer	Model: TRIMPOT 3386-F

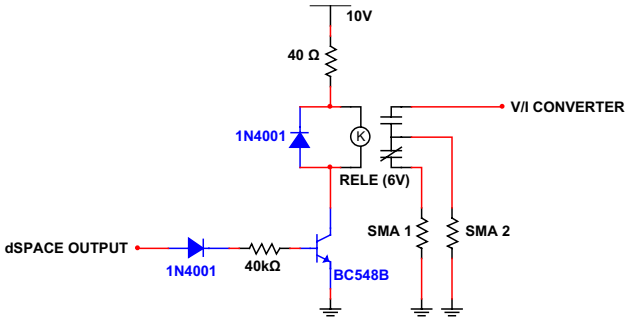

Fig. 16 Diagram of the electrical actuator

$-2°$, then rotates to $-5°$, and after that, it goes to angular position $\theta = 0°$.

As can be seen in Fig. 19, it clearly shown that using fuzzy controller, a low settling time for SMA is reached (around 2 s) as also an enhanced damping compared with on–off controller. For the latter, there is little damped characteristic of the airfoil, particularly in smaller angles, which remains after the transient response. According to Figs. 20 and 21, this characteristic is also verified for the steady-state errors as well its temporal derivative.

Using the on–off controller, a significant delay (6 s) of raise motion of the actual trajectory compared to that of the desired trajectory is seen. This is due to the fact that using an ordinary on–off controller, the fixed control voltage is generated only after some level of error is detected. The error and the derivative error have smaller fluctuation for the fuzzy controller. As shown in Figs. 20 and 21, the system can reach the desired position in less than 2 s and keep the steady state error less then 1 degree/s. The simulation results illustrate the effectiveness of the proposed fuzzy control algorithm for the position tracking.

Figure 22 shows the generated control voltage to the *V*/*I* converter. One can observed that with the application of fuzzy control, there was a reduction of approximately 50 % of the RMS value of *V* (1.64 V) with respect to the on–off control system that applied a constant voltage of 3.25 V.

Figure 23 shows the generated control voltage to the switching electric circuit (see Fig. 16) by the dSPACE board.

Both numerical and simulation results illustrate the effectiveness of the proposed fuzzy algorithm for the

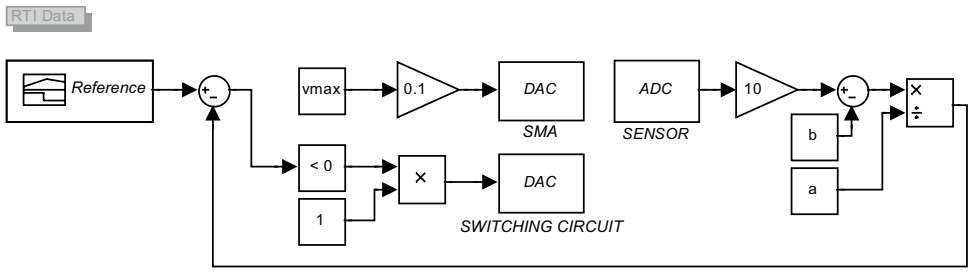

Fig. 17 Simulink® block diagram of the on–off control system

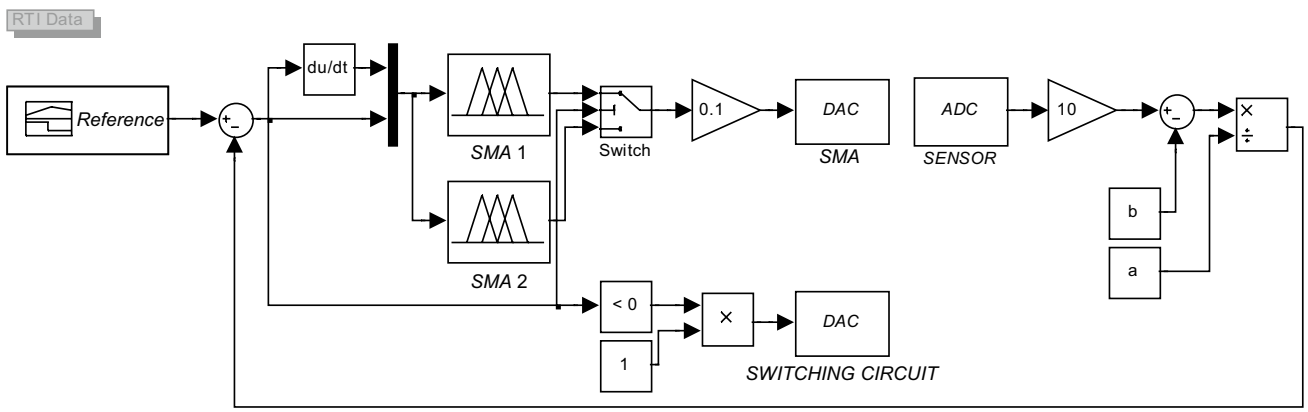

Fig. 18 Simulink® block diagram of the fuzzy control system

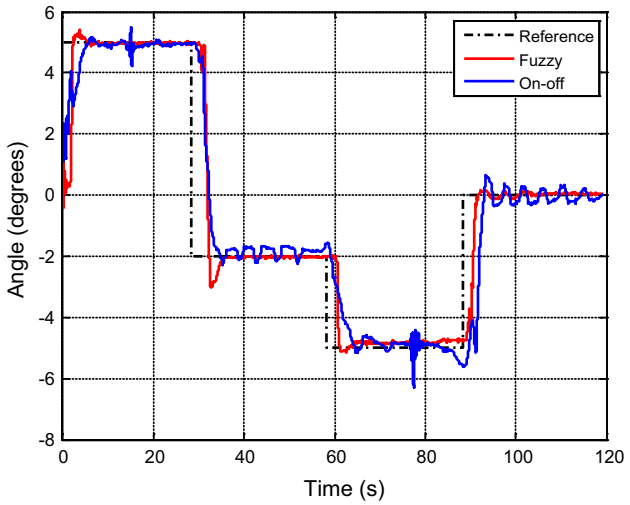

Fig. 19 Experimental angular responses of the sectioned airfoil using fuzzy and on–off controllers

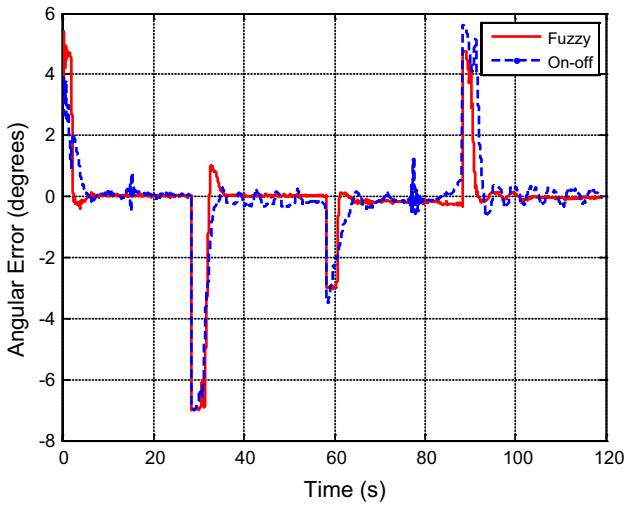

Fig. 20 Experimental angular error responses of the sectioned airfoil using fuzzy and on–off controllers

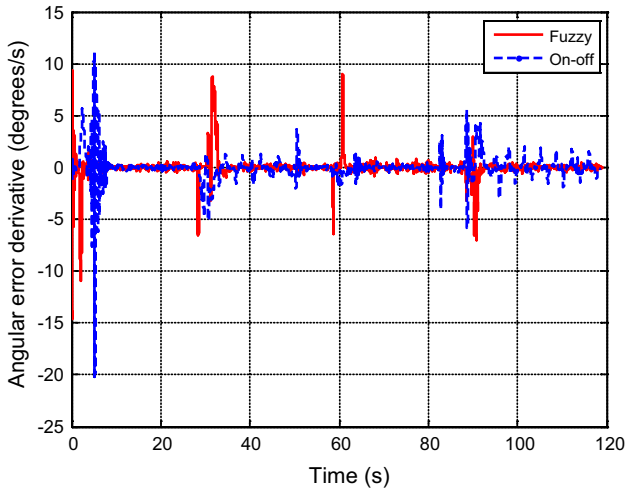

Fig. 21 Experimental angular error derivative responses of the sectioned airfoil using fuzzy and on–off controllers

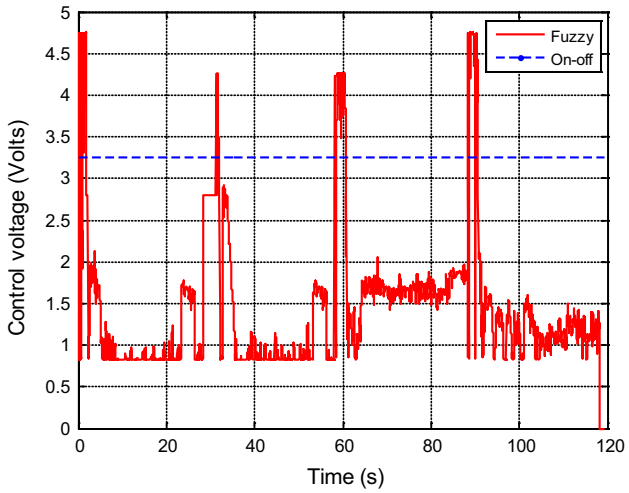

Fig. 22 Experimental control voltage applied to the *SMAs* actuators using fuzzy and on–off controllers

angular position control and provides an effective scheme for the experimental control of the considered sectioned airfoil profile.

6 Conclusions

A fuzzy controller has been developed to control the angular displacements of a sectioned airfoil actuated by a pair of SMA wires. The control system consists of a decentralized active angular control with local fuzzy controllers acting to each SMA actuator. The proposed fuzzy controller activates each of the wires using a pre-defined rule based on the angular position error and its first time derivative. The control strategy mimics the human learning process, requiring only minimal information on the environment.

Numerical and experimental tests were performed, which illustrated the effectiveness of the controller in tracking various angular trajectories of the sectioned airfoil. Experimental results for this real-time controller showed enhanced performances in both control voltage and response time over conventional on–off controller.

For future work, temperature sensors will be used to verify the thermal model and the influence of heating rate in SMA wires, and also to identify the main parameters of its mathematical model. Furthermore, in order to evaluate

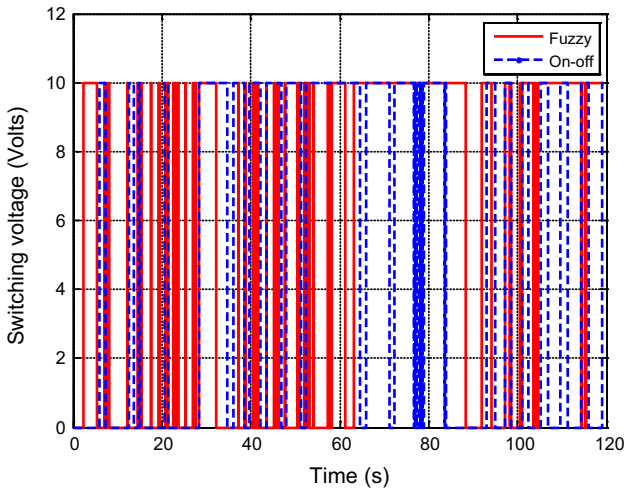

Fig. 23 Voltage applied to the switching electric circuit by the dSPACE board

the performance of the proposed fuzzy controller in a more complete way, the control system will be tested for other position waveforms (triangular and sinusoidal).

Acknowledgments The authors would like to thank FAPESP and also CNPq and FAPEMIG through INCT-EIE for the financial support of the reported research.

References

1. Barbarino S, Bilgen O, Ajaj RM, Friswell MI, Inman DJ (2011) A review of morphing aircraft. J Intell Mater Syst Struct 22:823–877
2. Barbarino S, Flores ELS, Ajaj RM, Dayyani I, Friswell MI (2014) A review on shape memory alloys with applications to morphing aircraft. J Intell Mater Syst Struct 23:1–19
3. Bil C, Massey K, Abdullah EJ (2013) Wing morphing control with shape memory alloy actuators. J Intell Mater Syst Struct 24(7):879–898
4. Brinson LC (1993) One-dimensional constitutive behavior of shape memory alloys: thermo-mechanical derivation with non-constant material functions and redefined martensite internal variable. J Intell Mater Syst Struct 4:229–242
5. De Breuker R, Abdalla MM, Gürdal Z (2011) A Generic morphing wing analysis and design framework. J Intell Mater Syst Struct 22:1025–1039
6. Driankov D, Hellendoorn H, Reinfrank M (1996) An introduction to fuzzy control. Springer, Berlin
7. Faria CT, Jr De Marqui C, Inman DJ, Jr Lopes V (2012) Nonlinear dynamic model and simulation of morphing wing profile actuated by shape memory alloys. Conf Proc Soc Exp Mech Ser 3:21–28
8. Feng Y, Rabbath CA, Hong H, Janaideh MA, Su CY (2010) Robust control for shape memory alloy micro-actuators based flap positioning system. American Control Conference, Baltimore, pp 4181–4186
9. Géoduin PA, Delaleau E, Bourgeot JM, Join C, Chirani SA, Calloch S (2011) Experimental comparison of classical PID and model-free control: position control of a shape memory alloy active spring. Control Eng Practice 19:433–441
10. Kannan S, Giraud-Audine CG, Patoor E (2013) Application of Laguerre based adaptive predictive control to shape memory alloy (SMA) actuator. ISA Trans 4:469–479
11. Ko J, Jun MB, Gilardi G, Haslam E, Park EJ (2011) Fuzzy PWM-PID control of cocontracting antagonistic shape memory alloy muscle pairs in an artificial finger. Mechatronics 21:1190–1202
12. Léchevin N, Rabbath CA (2005) Quasipassivity-based robust nonlinear control synthesis for flap positioning using shape memory alloy micro-actuators. American Control Conference, Portland, pp 3019–3024
13. Lee M (1990) Fuzzy logic in control systems: fuzzy logic controller—part I and II. IEEE Trans Syst Man Cybern 2:404–435
14. Lee J, Jin M, Ahn KK (2013) Precise tracking control of shape memory alloy actuator systems using hyperbolic tangential sliding mode control with time delay estimation. Mechatronics 23:310–317
15. Leo DJ (2007) Engineering analysis of smart material systems. Wiley, Hoboken
16. Lv H, Leng J, Du S (2009) A survey of adaptive materials and structures research in China. In: Proceedings of 50th AIAA/ASME/ASCE/ASH/ACS Structures, Structural Dynamics, and Materials Conference
17. Martin CA, Kudva J, Austin F, Jardine AP, Scherer LB, Lockyer AJ, Carpenter BF (1998) Smart materials and structures-smart wing volumes I, II, III, and IV. Report AFRL-ML-WP-TR-1999-4162. Northrop Grumman Corporation, Hawthorne
18. Paiva A, Savi MA (2005) An overview of constitutive models for shape memory alloys. Math Problems Eng 2006:1–30
19. Pankonien AM, Faria CT, Inman DJ (2013) Synergistic smart morphing aileron. In: Collection of Technical Papers—AIAA/ASME/ASCE/AHS/ASC Structures, Structural Dynamics and Materials Conference
20. Pankonien AM, Duraisamy K, Faria CT, Inman DJ (2014) Synergistic smart morphing aileron: aero-structural performance analysis. Chapter. doi:10.2514/6.2014-0924
21. Romano R, Tannuri EA (2009) Modeling, control and experimental validation of a novel actuator based on shape memory alloys. Mechatronics 19:1169–1177
22. Sofla AYN, Meguid SA, Tan KT, Yeo WK (2010) Shape morphing of aircraft wing: status and challenges. Mater Des 31:1284–1292
23. Stanewsky E (2001) Adaptive wing and flow control technology. Prog Aerosp Sci 37:583–667
24. Tai NT, Ahn KK (2012) A hysteresis functional link artificial neural network for identification and model predictive control of SMA actuator. J Process Control 22:766–777
25. Valasek J (2012) Morphing aerospace vehicles and structures. Aerospace series. Wiley, Hoboken
26. Zadeh LA (1965) Fuzzy sets. Inform Control 8(3):338–353